Effect on Microtubule Dynamics of XMAP230, a Microtubule-associated Protein Present in *Xenopus laevis* Eggs and Dividing Cells

Søren S. L. Andersen, Brigitte Buendia, Jorge E. Domínguez, Alan Sawyer, and Eric Karsenti

European Molecular Biology Laboratory, Cell Biology Program, D-69012 Heidelberg, Germany

Abstract. The reorganization from a radical interphase microtubule (MT) network into a bipolar spindle at the onset of mitosis involves a dramatic change in MT dynamics. Microtubule-associated proteins (MAPs) and other factors are thought to regulate MT dynamics both in interphase and in mitosis. In this study we report the purification and functional in vitro characterization of a 230-KD MAP from *Xenopus* egg extract (XMAP230). This protein is present in eggs, oocytes, testis and a *Xenopus* tissue culture cell line. It is apparently absent from non-dividing cells in which an immunologically related 200-kD protein is found. XMAP230 is composed of two isoforms with slightly different molecular masses and pIs. It is localized to interphase MTs, dissociates from MTs at the onset of prophase and specifically binds to spindle MTs during metaphase and anaphase. The dissociation constant of XMAP230 is 500 nM, the stoichiometry of binding to MTs is between 1:8 and 1:4, and the in vivo concentration is ~200 nM. Both isoforms are phosphorylated and have reduced affinity for microtubules in mitotic extracts. Analysis of the effect of XMAP230 on MT dynamics by video microscopy shows that it increases the growth rate, decreases the shrinking rate of MTs and strongly suppresses catastrophes. These results suggest that in vivo, XMAP230 participates in the control of the MT elongation rate, stabilizes MTs and locally modulates MT dynamics during mitosis.

At the onset of mitosis, microtubules (MTs)[1] reorganize from a radial network into a bipolar spindle. This reorganization involves a dramatic change in microtubule dynamics that allows the elimination of the interphase MTs and the growth of new highly dynamic MTs towards chromosomes. Both in interphase and mitosis, MTs originate from the centrosome and alternate between growing and shrinking phases at various rates (dynamic instability behavior, Kirschner and Mitchison, 1986). MT growth rates (v_g) and MT shrinking rates (v_s) are fairly similar in interphase and mitosis, but the frequency at which they transit from growth to shrinkage (catastrophe frequency, f_{cat}) increases ~10-fold during mitosis, and the opposite transition (rescue frequency, f_{res}) is reduced (Belmont et al., 1990; Gliksman et al., 1992; Verde et al., 1992). MTs grow much faster in vivo than in vitro at similar tubulin concentrations, and in vivo the value of f_{cat} is high, compared to that for pure MTs assembled in vitro (Walker et al., 1988). Clearly, a combination of microtubule-associated proteins (MAPs) and other factors regulate MT dynamics in vivo. Most of our knowledge of MAPs comes from studies on this type of molecule isolated from brain, that is, from non-dividing cells. Brain MAPs stabilize MTs, although video microscopy has only been used to study the mechanism by which they do this for tau and MAP2 (Drechsel et al., 1992; Pryer et al., 1992). In non-neuronal cells, the best characterized MAP is MAP4 (Parysek et al., 1984). Members of the MAP4 family have been found in mouse, rat and bovine cells (Parysek et al., 1984; Bloom et al., 1985; Murofushi et al., 1986). Early studies on the in vivo function of MAP4 have been limited to a demonstration of mitotic arrest in dividing HeLa cells injected with mAbs (Izant et al., 1983). Data from experiments using the antisense technique also indicate that MAP4 is required for normal progression through the cell cycle (K. R. Olson, and J. B. Olmsted, personal communication).

We know that the change in dynamics observed at the onset of mitosis is induced by the cyclin B-dependent kinase (Verde et al., 1990) but we still do not know the nature of the molecules involved in the regulation of MT dynamics both during interphase and mitosis in growing cells.

To identify proteins involved in mitotic spindle assembly, we are currently using *Xenopus* egg cytoplasmic extracts to systematically characterize different MAPs and generate reagents to study their function. We describe the purification and biochemical and functional characterization of XMAP-230, one of the *Xenopus* MAPs we have identified.

Brigitte Buendia's present address is Département de Biologie Supramoléculaire et Cellulaire, Institut J. Monod, UAR 9922, Tour 43, 75251 Cedex 05, France.

Address all correspondence to S. Andersen, EMBL, Postfach 10.2209, D-69012, Heidelberg, Germany. Tel.: 6221 387 323. Fax: 6221 387 306.

1. *Abbreviations used in this paper*: f_{cat}, catastrophe frequency; f_{res}, rescue frequency; MAP, microtubule-associated protein; MT, microtubule; v_g, growth rate; v_s, shrinkage rate.

Materials and Methods

Materials

Calf brain tubulin was prepared by two cycles of polymerization and depolymerization followed by phosphocellulose chromatography (Mitchison and Kirschner, 1984*a*,*b*). The tubulin we used was incompetent to assemble into MTs at concentrations below 30 μM. This was determined by video-enhanced interference contrast microscopy, cryo-electron microscopy, and turbidimetry. Human centrosomes were prepared from KE37 lymphoblasts according to Bornens et al. (1987). Unless indicated, chemicals were from Sigma Chem Co. (St. Louis, MO), Merck (Darmstadt, Germany), or Boehringer Mannheim GmbH (Mannheim, Germany).

Preparation of Xenopus Egg Extracts and Purification of XMAP230

Interphase extracts used for the purification of XMAP230 were prepared 90 min after activation of the eggs by an electric shock (12V, AC, 2S) according to Félix et al. (1993), with the following modifications. Protease inhibitors were added (10 μg/ml aprotinin, pepstatin, leupeptin, and 1 mM PMSF), the addition of an ATP regenerating system was omitted and the extracts were cleared by two centrifugations at 280,000 *g* for 40 min at 2°C before freezing in liquid nitrogen by 2-ml aliquots. 5 μM taxol (from a 10 mM stock in DMSO) was added to 20 ml thawed extract and incubated 15 min at 37°C. The taxol concentration was then raised to 20 μM, and after 5 min taxol stabilized brain MTs (5 μM final) were added to the extract. After 30 min at room temperature, the extract was loaded on a 40% sucrose cushion prepared in BRB80 (80 mM K-Pipes, 1 mM EGTA, 1 mM $MgCl_2$, pH 6.8) with protease inhibitors (1 mM PMSF, 2 μg/ml aprotinin, pepstatin and leupeptin), 5 μM taxol and 1 mM DTT, and centrifuged in a SW40 rotor at 80,000 *g*, 20 min, at 20°C. The pellet was resuspended in 1/4 of the original extract volume (5 ml) in CM buffer (100 mM K-Pipes, 0.5 mM EGTA, 2.5 mM $MgAc_2$, pH 7.0) with protease inhibitors, taxol, and DTT and centrifuged through a 40% sucrose cushion as above. The resulting pellet, consisting mostly of MAPs and tubulin, was resuspended in 1/10 of the original extract volume (2 ml) in CM buffer containing protease inhibitors, taxol, DTT, 300 mM NaCl + 10% glycerol, and incubated for 30 min at room temperature to elute MAPs. This was then centrifuged at 80,000 *g* for 30 min at 20°C in a TLA100.2 rotor. The supernatant (Smaps) was heated 7 min at 95°C, cooled 5 min on ice, and then centrifuged at 100,000 *g* for 30 min at 4°C in a TLA100.2 rotor. The supernatant was diluted fourfold with 100 mM piperazine, pH 5.5, 0.25 mg/ml pure BSA, protease inhibitors, DTT, and centrifuged in centricon-100 devices at 1000 *g* for 50 min at 4°C in a Heraeus Labofuge 200. The concentrated volume (1–2 ml) was pooled and loaded on a Mono-Q PC 1.6/5 SMART anion exchange column (Pharmacia LKB Biotechnology, Uppsala, Sweden) equilibrated with buffer A (A: 20 mM Piperazine, pH 5.5, 40 mM NaCl, protease inhibitors and DTT) at 100 μl/min at room temperature. A linear gradient from 0 to 25% B (B: 20 mM Piperazine, pH 5.5, 600 mM NaCl, protease inhibitors and DTT) was then performed in 1 ml. The concentration of B was linearly increased from 25 to 32% over 0.5 ml. A step increase in the concentration of B was then performed from 32 to 66% and XMAP-230 was immediately eluted from the column. The peak of XMAP230 eluted in 50 μl (fraction 24, see Fig. 1 *B*, lane 7) with an estimated buffer composition of 20 mM Piperazine, pH 5.5, 300 mM NaCl, protease inhibitors and DTT. Glycerol was added to the peak fraction (10% final) and XMAP-230 aliquoted by 3 μl and stored in liquid nitrogen. Nine different preparations of this protein were used throughout the work described in this article. The volumes and protein concentrations during a preparation of XMAP230 were typically as follows: the MAPs bound to MTs from 20 ml of a 280,000 *g* interphase egg extract (25–30 mg protein/ml extract) were eluted in 2 ml (2–3 mg protein/ml eluate). The purification yield was ~25% as estimated by comparing the intensity of the band revealed by immunoblotting of total 280,000 *g* extract with known amounts of pure 230-kD MAP. The peak fraction from the monoQ column contained 50 to 100 μg of pure XMAP230 in 50 μl (corresponding to 4–8 μM). We estimated the concentration of XMAP230 in the eggs to 200–300 nM by western blotting of mitotic extract and known amounts of XMAP230 from fraction 24. The staining intensity of the blots (probed with L5 and L7) were compared by densitometric scanning. The relative molecular mass of 230-kD was estimated from a curve derived from the mobility of MAP1A (350 kD), MAP1B (325 kD), MAP2 (270 kD), and myosin (200 kD) run as markers on 4% SDS-PAGE. Interphase (activated as described above) and CSF-arrested (mitotic) extracts used for MT regrowth off centrosomes and phosphorylation experiments were prepared as described by Murray (1991). The H1 kinase activities (Félix et al., 1993) in mitotic and interphase extracts were, respectively, 25 and 2 pmol/μl/min and the protein concentrations respectively 55 and 45 mg protein/ml extract.

Protein concentrations were measured according to (Bradford, 1976), using BSA as a standard. The concentration of pure XMAP230 was measured using a Micro BCA Protein Reagent Assay Kit (Pierce, BA oud-Beijerland, Holland), and BSA as standard.

Production of Monoclonal Antibodies

Total *Xenopus* MAPs were prepared as described above and separated on preparative 6% SDS-PAGE. After staining with Coomassie blue, the XMAP-230 band was cut and injected into mice (Galfrè, 1981). Fraction 24 from the monoQ column was used for the last injections. The antibodies were screened by immunoblot on *Xenopus* egg extract and by immunofluorescence on *Xenopus* cells. We obtained 2 IgG1 (Mouse-Hybridoma-Subtyping Kit Boehringer) mAbs named L5 and L7.

Dissociation Constant and Stoichiometry

Tubulin (200 μl, 10 mg/ml) precleared by centrifugation at 400,000 *g* for 10 min at 4°C in a TLA100 rotor was polymerized by adding taxol (Butner and Kirschner, 1991). XMAP230 (6 μl, 0.8 μM) was diluted in 144 μl of BRB80 containing 1 mM GTP and 20 μM taxol and centrifuged at 400,000 *g* for 10 min at 4°C in a TLA100 rotor. 50 μl of this supernatant were mixed with 50 μl of taxol stabilized MTs, the mixture incubated for 10 min at 37°C and centrifuged through a 4 M glycerol cushion under preclearing conditions. Supernatant and pellet were processed for SDS-PAGE. The dissociation constant was determined by varying MT polymer concentration between 10^{-7} and 10^{-5} M. The ratio of XMAP230 to tubulin polymer concentration never exceeded 1:6 in order not to saturate MTs. To determine the stoichiometry of binding, taxol MTs were resuspended at a concentration of 4 μM. They were then mixed with an equal volume of buffer containing XMAP230 at increasing concentrations. After a 10-min incubation at 37°C MTs were separated from the MAP by centrifugation under pre-clearing conditions. XMAP230 in the supernatants and pellets was quantified by densitometric scanning of silver stained gels.

Immunofluorescence

Xenopus XL177 cells (Miller and Daniel, 1977), were grown in Liebowitz L-15 (GIBCO BRL, Gaithersburg, MD) containing 15% FBS, at room temperature. The cells were seeded on glass coverslips for immunofluorescence studies. The cells were fixed in methanol and immunofluorescence was carried out as previously described (Bré et al., 1987). Primary antibodies: Rabbit anti-tubulin Ab raised against the terminal 13 amino acids of tubulin (a gift from T. Kreis, University of Geneva, Geneva, Switzerland). The 125 monoclonal anti-MAP1B antibody (IgM) was a gift from Ulloa et al. (Ulloa et al., 1993*a*,*b*). The L5 and L7 delipidated ascites were used, respectively, 1/20 and at a 1/5,000 dilution. Secondary antibodies (Dianova GmBH, Hamburg, Germany) were: Fluorescein-labeled donkey anti-rabbit and Texas red-labeled donkey anti-mouse diluted respectively 1:100 and 1:50. Antibodies were diluted in PBS with 3% BSA, 0.05% Triton X-100, 20 mM NaN_3.

Video Microscopy

We used video-enhanced contrast, differential interference contrast (AVEC-DIC, Allen et al., 1981) microscopy to follow MT dynamics as described below and in more detail by Chrétien, D., S. D. Fuller, and E. Karsenti, manuscript submitted for publication.

Homemade observation chambers with a theoretical volume of 10 μl and a total surface area exposed to buffer of ~0.25 cm^2 were used. The tubing needed for injection increased the actual volume to 25 μl. The 12-mm round glass coverslips used to close the chambers (Fisher Scientific, Pittsburgh, PA) were cleaned with ethanol and wiped dry with Kleenex before mounting. Tubulin was thawed at 37°C and centrifuged at 14,000 g for 10 min at 4°C immediately before use. Tubulin at the desired concentration was mixed with centrosomes (~3×10^3/μl) at 4°C in an Eppendorf tube and then injected into a chamber followed by 7-min incubation on ice. The chamber was then washed with 300 μl cold tubulin at the desired concentration and placed on the stage of a Zeiss Axiovert 10 photomicroscope (Zeiss GmbH, Oberkochen, Germany). Stage, condenser and lens were heated to 37°C (precise temperature control). The working temperature inside the chamber was 35°C (measured with a thermo-couple). The chamber was injected with 2.5 μl of XMAP230 (fraction 24) or 2.5 μl of control buffer (20

mM piperazine, 300 mM NaCl, 10% glycerol, pH 5.5) and the timer was started. v_g and v_s were estimated by measuring changes in length of individual MTs over intervals varying from 1–30 s. The samples were observed for no longer than 40 min. In the presence of XMAP230 the measurement of individual MTs was difficult due to the high number of MTs growing from the centrosome and because of increased lateral movement as compared to the control; In the presence of XMAP230 v_g and v_s were therefore also measured by the change in radius of the circle formed by the ends of the growing MTs (Fig. 7 *B*); This "bulk" v_g/v_s was equal to the v_g/v_s of individual MTs. For dynamic MTs, the f_{cat} was determined by dividing the total number of catastrophes observed, by the total time spent in the growing phase. v_s was determined by depleting the chamber of tubulin after 20 min of growth by perfusion of 300 μl BRB80, 1 mM GTP, prewarmed at 35°C. The exchange in the chamber took 10 s, followed by immediate injection of either 2.5 μl XMAP230 (fraction 24) or 2.5 μl control buffer.

The microscope and image acquisition were described previously (Verde et al., 1992). MT dynamics were analyzed on a Macintosh Quadra 800 using NIH-Image 1.50 and Kaleidagraph 3.0 programs.

Calculations

From the K_d, it is possible to calculate the amount of bound and unbound XMAP230 at any concentration of MTs and XMAP230 using the following equation in which: K_d is the molar dissociation constant of XMAP230 from MTs, *mx* is the molar concentration of the complex between MTs (*m*) and XMAP230 (*x*), *m* is the total molar concentration of MTs and *x* is the total molar concentration of XMAP230:

$$mx = \frac{1}{2}(Kd + m + x) - \sqrt{\frac{1}{4}(Kd + m + x)^2 - m \cdot x} \quad (1)$$

In the experiments reported here, we had ~100 centrosomes per chamber. If we assume that each nucleates 100 MTs with a length of 10 μm, the tubulin dimer being 8 nm in length and the volume of the chamber 25 μl, *m* was ~11 pM. The concentration of *x* was varied between 0.4 and 0.8 μM. Using Eq. 1 we find that the molar concentration of *mx* must have been between 0.4 and 0.55 pM in these experiments. This gives a *mx*:*m* ratio between 1:2.3 and 1:1.6. With a stoichiometry (maximum *mx*:*m* ratio) between 1:4 and 1:8 this means that in our in vitro experiments the MTs were saturated with XMAP230.

Microtubule Spin-down with Pure XMAP230

Tubulin (5 mg/ml) was centrifuged at 70,000 *g* for 10 min at 4°C in a TLA100 rotor. The supernatant was diluted to 3 mg/ml with BRB80-glycerol (160 mM Pipes, 2 mM EGTA, 10 mM $MgCl_2$, 1 mM GTP, 66% glycerol) and MTs polymerized for 30 min at 37°C. MTs were then diluted 1:1 with BRB80-taxol (BRB80 with 20 μM taxol). 2 μl of pure XMAP230 (at 6 μM) were added to 8 μl MTs at 15, 1.5, 0.15 μM final MT concentrations and incubated 30 min at room temperature. MTs were then fixed for 10 min with 1 ml of 0.5% glutaraldehyde in BRB80 and diluted to 30 pM in BRB80. 1 ml of the suspension was spun on coverslips and examined by immunofluorescence according to Evans et al. (1985).

Preparation of Tissue Extracts

Organs were removed from anesthetized frogs at 4°C and transferred to liquid nitrogen. The organs were pulverized with a mortar in liquid nitrogen and Dounce homogenized in CM buffer with protease inhibitors for 1 min at 0°C and processed for SDS-PAGE.

Labeling of XMAP230 with [γ-P^{32}]ATP

1 μCi [γ-P^{32}]ATP was added per μl of mitotic and interphase extract.

Samples were incubated 15 min at room temperature and then diluted with 2 vol XB (Murray, 1991) and immediately boiled 5 min at 95°C, followed by 5 min on ice. The samples were centrifuged at 100,000 *g*, 30 min, 2°C in a TLA100 rotor and processed for 2-D gel electrophoresis.

Gel Electrophoresis and Western Blots

SDS-PAGE was performed according to the procedure of (Laemmli, 1970) using a Mini-Protean II Dual Slab Cell system (Bio Rad Labs., Hercules, CA). IEF was performed using a Mini-Protean II 2-D Cell system (Bio Rad Labs.). Molecular mass markers were High and Low molecular mass markers from Bio Rad Labs. Transfer to nitrocellulose was performed in a semi-dry blotting apparatus (Bio Rad Labs.). Blocking, primary and secondary antibody incubations were done according to the IntenSE BL (Amersham Corp., Arlington Heights, IL) enhancement kit. Fig. 5 *B* was developed using ECL (Amersham Corp.).

Results

Purification of XMAP230 from Xenopus Egg Extract

Using a mAb directed against rat MAP1B (Ulloa et al., 1993*a*,*b*) we identified a 230-kD protein in total *Xenopus* egg extracts (not shown). We decided to purify this protein to further characterize its function. In preliminary experiments, this protein was found to coprecipitate with MTs after addition of taxol to the extract and to be eluted by 0.3–0.4 M NaCl. We therefore used affinity purification of the 230-kD protein on MTs as a first step in the procedure. Fig. 1 *A* shows the proteins that bind to taxol MTs from a 280,000 *g* interphase *Xenopus* egg extract under the conditions described in Materials and Methods. Fig. 1 *B* shows the purification steps. The 230-kD protein is thermostable, and the proteins remaining after boiling the eluted MAPs at 95°C are shown in Fig. 1 *B*, lane *4*. We followed the 230-kD protein during the purification by immunoblotting with the anti-MAP1B mAb (Fig. 1 *C*). The MAP1B antibody strongly stained the thermostable 230 kD protein (Fig. 1 *C*, lane *4*), which we further purified with anion exchange chromatography (Fig. 1, *B* and *C*, lane *7*). The pure 230-kD protein was still able to bind MTs as shown by immunofluorescence using the MAP1B mAb (Fig. 1, *D* and *E*). It associated with MTs along their entire length, and we observed the formation of some MT bundles in the presence of this MAP (Fig. 1, *D* and *E*, *arrowheads*). We estimated the concentration of the 230-kD MAP in eggs at 200–300 nM (Materials and Methods). We name the 230-kD MAP, XMAP230 for *Xenopus* MAP of 230 kD.

XMAP230 is Composed of Two Related Isoforms

While screening mAbs raised against the purified protein, we obtained two clones (named L5 and L7), that recognized XMAP230 on western blots (data not shown). However, the L5 mAb stained a protein of slightly lower apparent molecular mass (~230 kD) than the L7 (~235 kD) mAb (data not shown). This suggested that XMAP230 was not one but at least two different proteins or isoforms. L5 and L7 did not recognize phosphorylated epitopes, because treatment of the blots by alkaline phosphatase prior to incubation with the antibodies did not reduce the signal (data not shown); The signal given by the anti-MAP1B mAb which recognizes a phospho-epitope (Ulloa et al., 1993*b*) was as expected completely abolished (data not shown). These data indicated that the L5 and L7 mAbs recognized XMAP230 independently of its phosphorylation state.

A 2-D gel electrophoresis analysis of XMAP230 confirmed that it was composed of two separate isoforms (Fig. 2, *A* and *B*) having a pI between 4.3 and 4.7 (Fig. 2 *B*); One protein was slightly more acidic and had a slightly higher apparent molecular mass than the other. The more acidic high molecular mass protein was recognized by the L7 whereas the other protein was recognized by the L5 mAb only (Fig. 2 *A*). Peptide mapping revealed that the L5 and the L7 proteins were strongly related (data not shown). We will refer

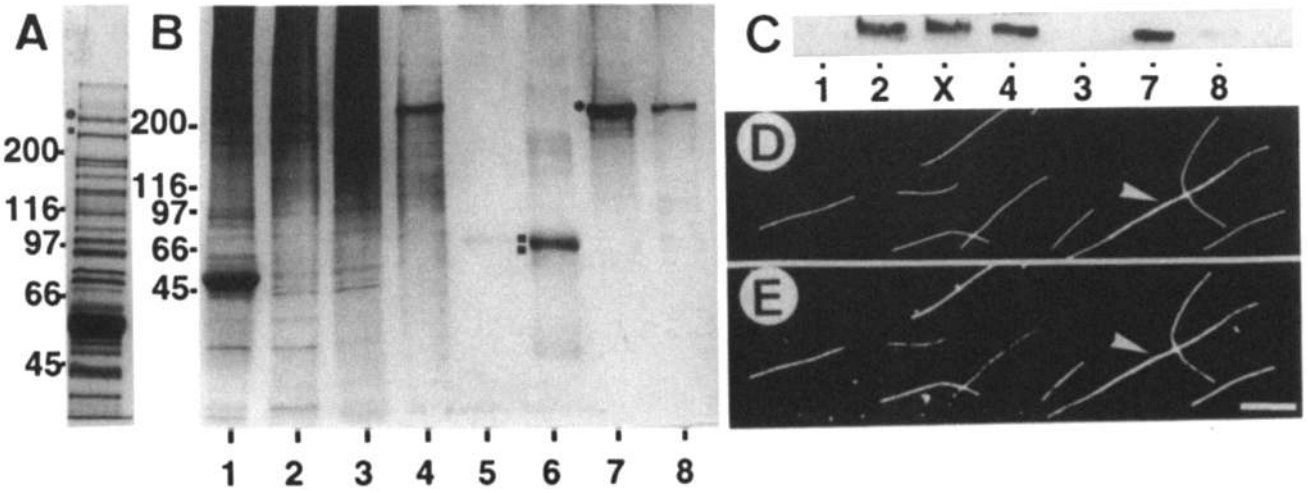

Figure 1. Purification of XMAP230. (*A*) Total MAP fraction with MTs; The star indicates XMAP230 and the rectangle a MAP with a molecular mass similar to that of XMAP215 (Gard and Kirschner, 1987). (*B*) Purification steps; lane *1*, pellet after elution of MAPs; lane *2*, MAPs eluted from MTs with 300 mM NaCl in CM buffer; lane *3*, MAP pellet after 7 min at 95°C; lane *4*, MAP supernatant after 7 min at 95°C; lane *5*, Centricon-100 flow-through; lane *6*, mono-Q column flow-through (*two rectangles* indicate BSA added before concentration on Centricon-100); lane *7*, mono-Q peak fraction of XMAP230 (fraction 24) eluted at 300 mM NaCl; the volume of fraction 24 was 50 μl and fraction 24 was used in all subsequent experiments; lane *8*, fraction 25 contains some low molecular mass contaminating proteins. The same volume of sample was loaded in lanes *1–6* and ten times less in lanes *7* and *8*. (*C*) Western blot with a mAb against a phosphorylated epitope of rat MAP1B; lane *X*, total MAP fraction with MTs; The other lanes as in *B*. *D* and *E* XMAP230 binds along the entire length of taxol stabilized MTs and occasional bundles are formed; after incubation with XMAP230, MTs were fixed with glutaraldehyde and double-stained with (*D*) a polyclonal rabbit anti-tubulin antibody and (*E*) the anti-MAP1B mAb; the arrowhead indicates a MT bundle and the bar 5 μm. *A* is a 6% silver stained SDS-PAGE. *B* is a 4–15% silver-stained SDS-PAGE. Molecular mass markers are indicated.

to the proteins recognized by L5 and the L7 mAbs as XMAP230 unless it is essential to make the distinction, in which case we will call them XMAP230a (L7, higher molecular mass) and XMAP230b (L5, lower molecular mass).

XMAP230 Is Expressed in Eggs, Oocytes, Testis and Growing Tissue Culture Cells but Not in Non-dividing Cells

We tested the expression pattern of XMAP230 in different *Xenopus* tissues using the L5 and the L7 mAbs (Fig. 3, only L7 labeling is shown). XMAP230 was only present in eggs, oocytes, testis and in the XL177 tissue culture cell line (Miller and Daniel, 1977). In brain, heart, lung, stomach and muscle, the mAbs recognized a 200-kD protein but not XMAP230. The same result was obtained with both antibodies. This suggests that the expression of XMAP230 is restricted to tissues containing cells capable of undergoing frequent cell division and that an immunologically related protein of lower molecular mass is present in non-dividing cells.

Localization of XMAP230 During the Cell Cycle

We used *Xenopus* XL177 cells to probe the localization of XMAP230 during the cell cycle (Fig. 4). The L5 and the L7 mAbs gave identical staining patterns. Fig. 4 shows cells probed with the L7 mAb. In prophase, there was a diffuse cytoplasmic staining and no MT staining although the MT network was still intact (Fig. 4, *A–C*). However, areas with high MT density (like the MTOCs) were stained. At metaphase/early anaphase XMAP230 was localized to the mitotic spindle, but astral MTs were not labeled (Fig. 4, *D–F*). This staining pattern persisted during anaphase (Fig. 4, *G–I*). In telophase, astral MTs and the mid-zone and midbody MTs became heavily stained (Fig. 4, *J–O*). In cells in interphase, XMAP230 was localized on the MT network (Fig. 4, *P–R*).

XMAP230 is Phosphorylated and Binds Weakly to MTs in Mitotic Egg Extracts

We thought that hyperphosphorylation could account for the dissociation of XMAP230 from MTs in prophase and from the astral microtubules during metaphase. To test this, we added [γ-P^{32}]ATP to interphasic and mitotic egg extracts, heated to remove non-thermostable proteins, and examined the phosphorylation level of XMAP230 by 2-D gels and autoradiography. The protein recovered from interphasic extracts was clearly resolved in two weakly labeled isoforms (Fig. 5 *A*, *I*). The spot seen ~200-kD on this gel is a contaminant thermostable protein. The protein recovered from the mitotic extract was resolved into one strongly labeled spot that showed an acidic shift of 0.25 pI units compared to the interphasic form of the protein (Fig. 5 *A*, *I* and *M*). Both isoforms were phosphorylated in the mitotic extract and they migrated close to each other so that it became hard to distinguish them (data not shown). XMAP230 was completely absent from the pellet of MAPs prepared from mitotic extracts and remained in the supernatant showing a strong upshift (Fig. 5 *B*). We examined the binding of XMAP230 to MTs nucleated by centrosomes in mitotic extracts by immunofluorescence, using both the L5 and L7 mAbs. Single MTs were not stained in the mitotic extract although some MT bundles were. In the interphase and 6-DMAP treated mitotic extract all MTs were strongly

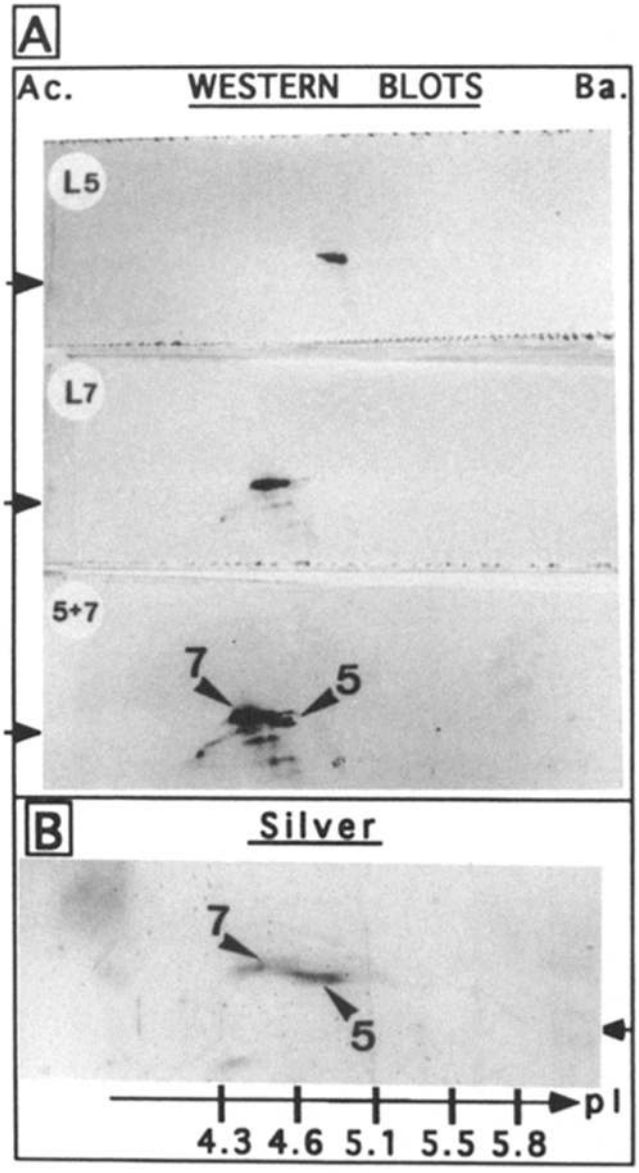

Figure 2. XMAP230 is composed of two polypeptides. (*A*) Western blots of 2-D gels (the second dimension was 6% SDS-PAGE); *L5* indicates staining with the L5 mAb, *L7* indicates staining with the L7 mAb; *5+7* indicates that the blot was first stained with the L7, developed, and then stained with the L5 mAb; The arrowheads labeled 5 and 7 indicate the proteins recognized by the L5 and the L7 mAb, respectively. (*B*) Silver stained 2-D gel (the second dimension was 4% SDS-PAGE) showing the pI of XMAP230 prepared from extracts in interphase; The arrowheads labeled *5* and *7* indicate the proteins recognized by the L5 and the L7 mAb respectively; *Ac* and *Ba* indicate, respectively, the acidic and the basic end of the first dimension IEF gel; samples loaded on the gels were from the heat stable fraction of a 280,000 *g* extract supernatant; the pI scale was established using Pharmacia's carbamylated carbonic anhydrase.

stained (data not shown, 6-DMAP is a non-specific kinase inhibitor [Neant and Guerrier, 1988; Verde et al., 1990]).

Stoichiometry of Binding and Affinity for Microtubules of XMAP230

To determine the stoichiometry of binding of XMAP230 to

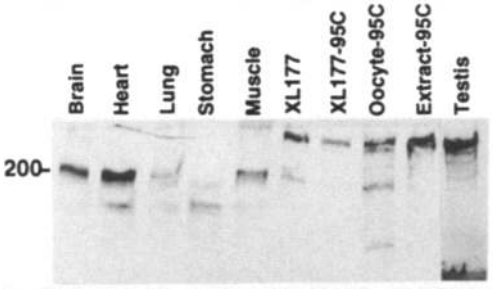

Figure 3. Western blot of *Xenopus* tissues probed with the L7 mAb. The samples were run on 6% SDS-PAGE; The same amount of total protein was loaded in all lanes. "*95C*" indicates that the heat stable fraction of total protein was loaded in that lane. The position of the 200-kD molecular mass marker is indicated.

MTs we chose a concentration of taxol stabilized MTs of 2 μM, added increasing concentrations of XMAP230 to the suspension and looked for the appearance of XMAP230 in the supernatant, indicating saturation of the MTs with the MAP. Saturation occurred between 0.25 and 0.50 μM XMAP230 (Fig. 6 *A*). At higher molar ratios, the amount of XMAP230 present in the supernatant increased in proportion to the amount of MAP added. Therefore, saturation occurred at a molar ratio of XMAP230 to tubulin dimer between 1:8 and 1:4 (Fig. 6 *A*). This is in the same range as the ratio reported for tau (1:5) (Hirokawa et al., 1988) but different from MAP1A (1:12) (Hirokawa et al., 1988).

We also determined the dissociation constant (K_d) of XMAP230, which is given by the polymer concentration at which half of the protein is bound to MTs. As shown in Fig. 6 *B*, all the protein was bound to microtubules at 1 μM and none at 0.1 μM. A closer inspection in the 0.1 and 1.0 μM range showed that equimolar distribution between pellet and supernatant occurred at 0.5 μM tubulin (data not shown). We conclude that the value of the K_d is close to 500 mM, which is similar to that reported for tau (Butner and Kirschner, 1991).

Effect of XMAP230 on the Parameters of Microtubule Dynamic Instability

We first examined the effect of XMAP230 on the spontaneous assembly of bovine brain tubulin. XMAP230 at the highest concentration we could assay (0.8 μM) and at 10 μM tubulin did not stimulate spontaneous assembly (data not shown). The effect of XMAP230 on microtubule dynamics was then investigated on centrosome-nucleated MTs by video microscopy. Typical asters produced in this way are shown in Fig. 7 *A*. At the tubulin concentration used (11 μM), MTs grew at a rate of 1.4 μm/min and showed occasional catastrophes (Fig. 7 *A*, *bottom*). Addition of XMAP230 at 0.6 μM resulted in an increase in v_g by a factor of 2 to 4 compared to the control MTs, depending on the batch of protein used (Fig. 7, *A* and *B* and Table I). The concentration in the chamber gives the molar ratio of total XMAP230 to soluble tubulin. However, the important ratio is that of MT bound XMAP230 to tubulin polymer. We calculated that MTs were saturated by XMAP230 in these experiments (Materials and Methods). If XMAP230 was diluted below

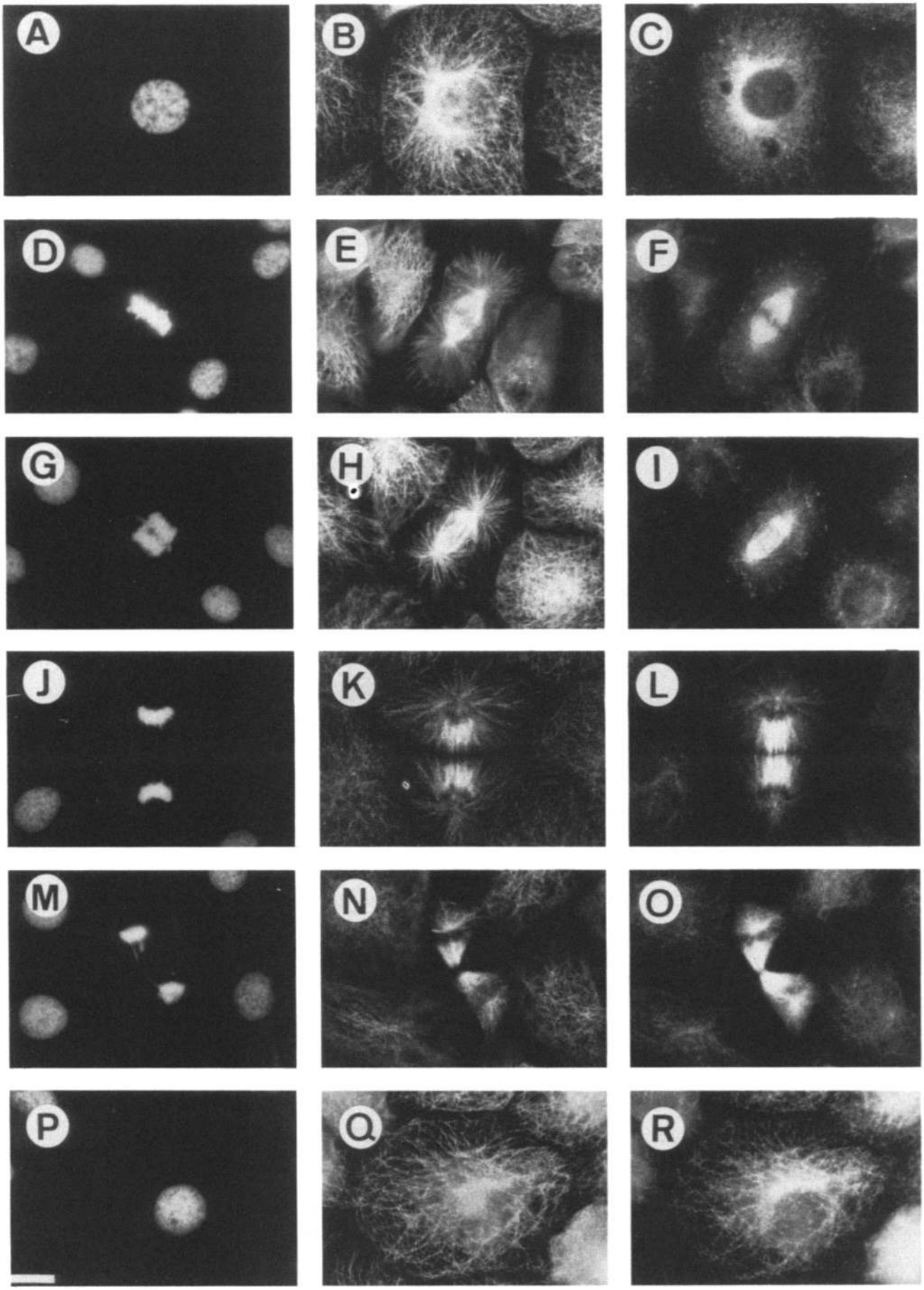

Figure 4. XMAP230 localization in XL177 cells during the cell cycle. XL177 cells (Miller and Daniel, 1977) were stained with: Hoechst (*A*, *D*, *G*, *J*, *M*, and *P*), a rabbit anti-tubulin primary antibody and a secondary FITC conjugated donkey anti-rabbit antibody (*B*, *E*, *H*, *K*, *N*, and *Q*), the L7 mAb as primary and a secondary Texas red conjugated donkey anti-mouse antibody (*C*, *F*, *I*, *L*, *O*, and *R*). Prophase (*A–C*), metaphase/early anaphase (*D–F*), anaphase (*G–I*), late anaphase (*J–L*), telophase (*M–O*) and interphase (*P–R*). Bar, 10 μM.

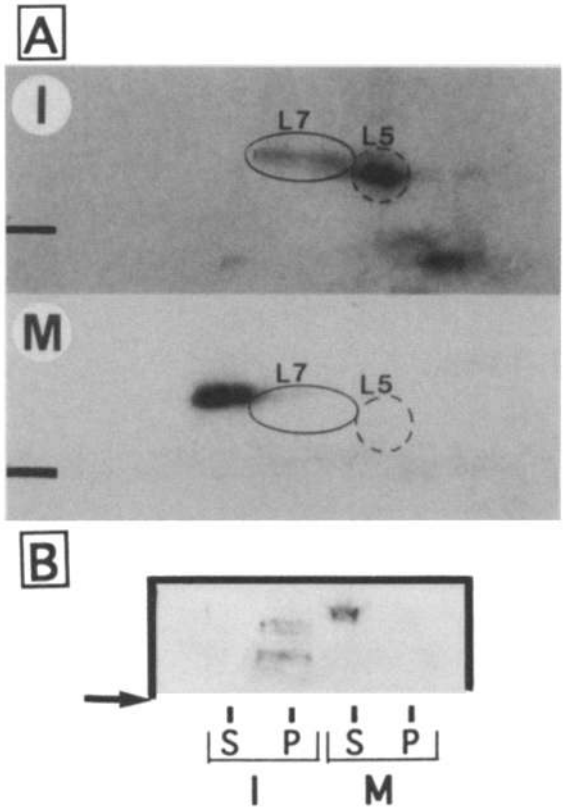

Figure 5. Phosphorylation of XMAP230 and the effect on binding to MTs in egg extracts. (*A*) Autoradiograms of 2-D gels (the second dimension is 4% SDS-PAGE) of P^{32}-labeled XMAP230 prepared from extracts in Interphase *I* and Mitosis *M*; *I* is a 7- and *M* a 2-d exposure; The position of the *L5* and the *L7* isoforms is indicated on both gels. The acidic end is to the left and the basic end is to the right. Samples loaded on the gels were from the heat stable fraction of a 280,000 *g* extract supernatant. (*B*) Western blot (4% SDS-PAGE stained with both L5 and L7) of MAPs prepared from extracts in Interphase, *I* or Mitosis, *M*; *P* denotes the MT pellet with MAPs and *S* the remaining supernatant. Arrow indicates the 200-kD molecular marker. Note the strong upshift of the protein from the mitotic extract. Bar indicates the 200-kD molecular marker.

saturation, there was no observable effect on MT dynamics (data not shown). We conclude that XMAP230 does increase v_g slightly, although this is not a dramatic effect.

As shown in Fig. 7, pure MTs undergo catastrophic depolymerization and XMAP230 completely suppressed the occurrence of such catastrophes. However, since MTs also grew faster in the presence of XMAP230, it was possible that the elimination of catastrophes was due to the higher v_g. To test the effect of XMAP230 on f_{cat}, the experiments were repeated at similar v_gs. In the presence of control buffer and at 10 μM tubulin, f_{cat} was 0.47 min^{-1} and v_g was 1.2 μm/min (Table II). At 6 μM tubulin in the presence of XMAP230, v_g was similar (1.1 μm/min) and f_{cat} equal to zero (Table II). At 6 μM tubulin, in the absence of XMAP-230, f_{cat} was so high that only a few, very short, MTs were actually observed to grow off centrosomes, making measurements difficult (data not shown). It is interesting to note that many more MTs were nucleated in the presence of XMAP230 than in its absence (Fig. 7 *A* and *B*). This is probably due to the suppression of f_{cat} by XMAP230 because we also observed this phenomenon under conditions where the growth rates were identical (data not shown).

Since no catastrophes were observed in the presence of XMAP230, we could not determine its effect on v_s after a spontaneous transition to the shrinkage phase. Walker et al. (1991) showed that v_s is the same whether induced by dilution or by spontaneous transition into the shrinking phase. The shrinkage rate was therefore determined after perfusion of buffer into the chamber (see Materials and Methods). MTs started to shrink immediately after perfusion (Fig. 8, *A* and *B*). In the presence of XMAP230 the shrinkage rate was approximately 6-fold lower than in the absence of the protein (Fig. 8 and Table II). The decrease in v_s was dependent on the continuous presence of XMAP230 (Fig. 8 *B*). MTs grown in the presence of XMAP230, and perfused by buffer lacking the MAP, had the same v_s as control MTs (data not shown). This is an expected result in view of the dissociation constant of XMAP230 for MTs.

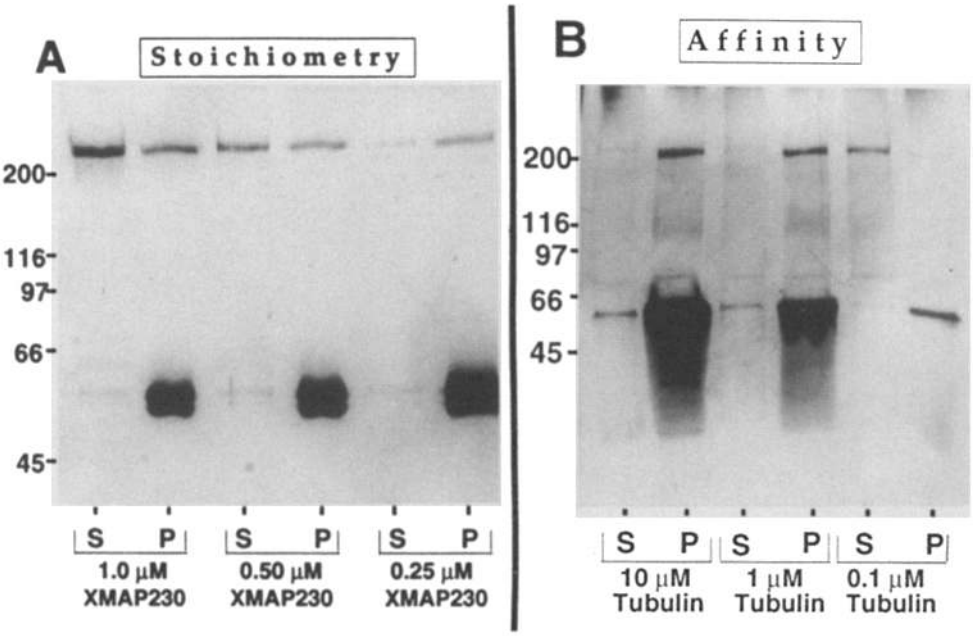

Figure 6. Stoichiometry and affinity of XMAP230 for MTs. (*A*) Stoichiometry; pure MTs (2 μM final concentration) were incubated with increasing concentrations of XMAP230 (indicated below the gel) and centrifuged as described in Materials and Methods; XMAP230 saturates MTs at a stoichiometry between 1:4 and 1:8. (*B*) Affinity; XMAP230 at constant concentration (16 nM) was incubated with MTs at variable concentrations (indicated below the gel) and centrifuged as described in Materials and Methods. *S*, supernatant, *P*, MT pellet. *A* and *B*, respectively, 7.5% and 4–15% silver-stained gels. Molecular mass markers are indicated.

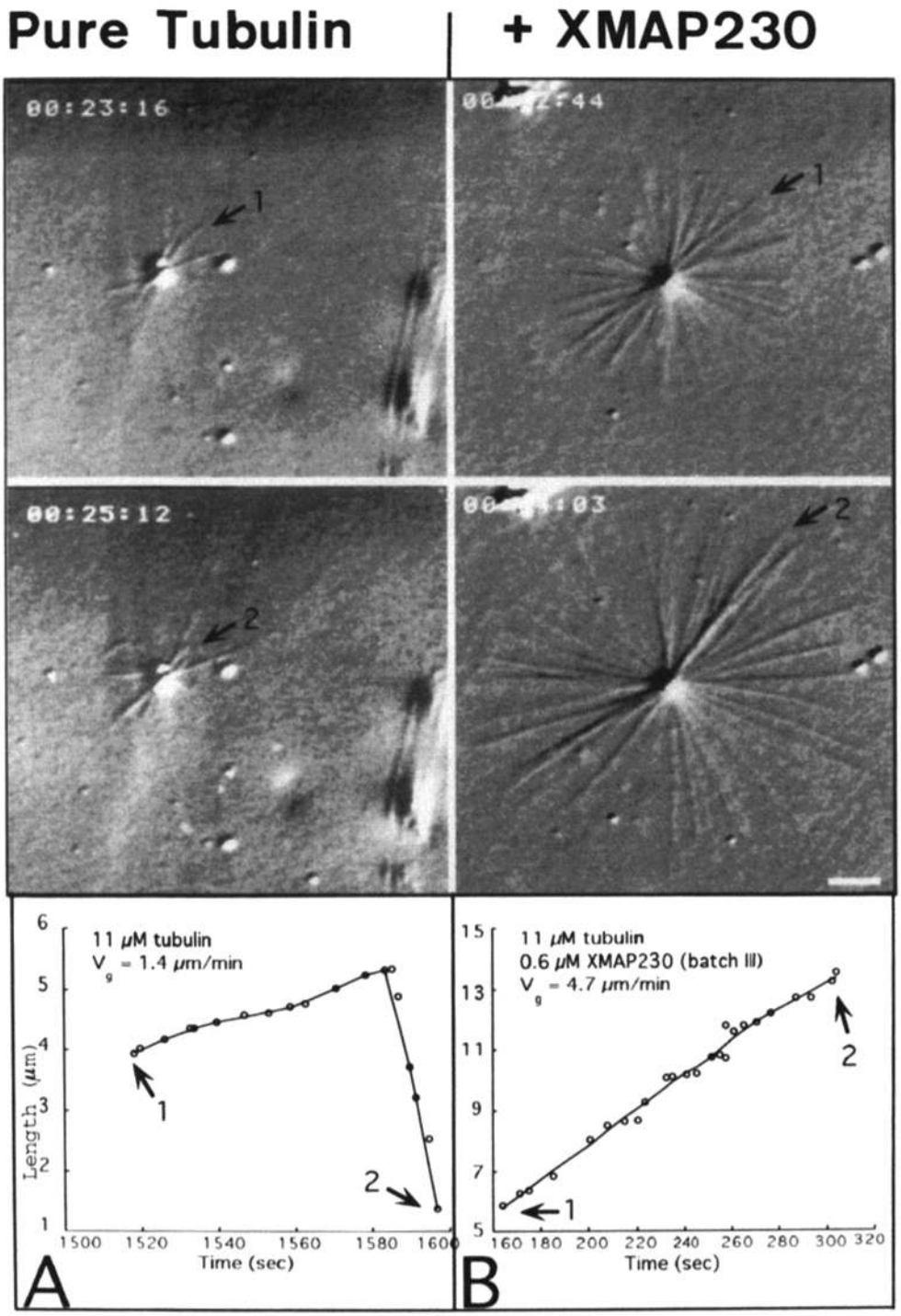

Figure 7. XMAP230 increases v_g (see Table I). (*A*) Control experiment; MTs grown off centrosomes in the presence of 11 μM tubulin are seen after 23 min, 16 s (top left) and 25 min, 12 s (middle left) of growth; The growth, catastrophe and shrinkage of one representative MT in that time interval, are shown (bottom left, *arrows 1* and 2 indicate this MT in each panel). (*B*) MTs grown off centrosomes in the presence of 11 μM tubulin together with 0.6 μM XMAP230 are seen at 2 min, 44 s (*top right*) and 4 min, 3 s (*middle right*); the growth of one representative MT in that time interval is shown (*bottom right*). Bar, 4 μm.

Table I. V_g Is Increased Two- to Fourfold in the Presence of XMAP230

μM tubulin	8	8	8	8	8	11	11
μM XMAP230, batch	0.7,I	0.8,II	0.6,III	0.4,IV	C	0.6,III	C
$v_g \pm s_d$ (μm/min)	3.5 ± 0.3	2.3 ± 0.3	1.5 ± 0.3	1.9 ± 0.3	0.9 ± 0.4	4.7 ± 0.8	1.4 ± 0.3
No. of MTs	7	8	6	12	11	11	8

The experiments were performed with 8 or 11 μM tubulin in a chamber at 35°C with BRB80 + 1 mM GTP (Materials and Methods); the concentration and batch of XMAP230 inside the video chamber is indicated; *batch* denotes that XMAP230 from different purifications was used; *C* indicates that control buffer was added instead of XMAP230; v_g is the average growth rate of MTs (measured as indicated in Fig. 7); s_d is the standard deviation of the average v_g; *No. of MTs* is the number of measured MTs.

Table II. XMAP230 Suppresses Catastrophes and Decreases v_s Sixfold

μM tubulin	6	10	10	14
μM XMAP230, batch	0.5,V	C	0.5,V	C
$v_g + s_d$ (μm/min)	1.1 ± 0.3	1.2 ± 0.2	–	–
f_{cat} (s^{-1})	n.o.	0.008	–	–
$v_s \pm$ sd (μm/min)	–	–	1.7 ± 0.9	10.5 ± 3.0
No. of MTs	13	16	9	7

The experiments were performed in a chamber at 35°C with BRB80 + 1 mM GTP (Materials and Methods); the tubulin concentration, concentration and batch of XMAP230 inside the video chamber are indicated. In the experiments concerning f_{cat}, MTs were grown at the same growth rate in the presence or absence of XMAP230 (see text for more detail) and the f_{cat} values were obtained over a total time of MT growth of 74 min (6 μM tubulin) and 93 min (10 μM tubulin). In the experiments concerning v_s, MTs were grown until the aster reached a diameter of ~30 μm in the presence or absence of XMAP230; Shrinkage was then induced by perfusion with buffer, and XMAP230 or control buffer added immediately thereafter (as indicated in Fig. 8 *B*). *sd* is the standard deviation of the average v_g or v_s, f_{cat} is the frequency of catastrophes; *n.o.* denotes that no catastrophes were observed; *No. of MTs* is the number of measured MTs.

Discussion

XMAP230 and Other MAPs

XMAP230 is most likely the same as the p220 protein purified by Shiina et al. (1992), because we did not find other thermostable MAPs in *Xenopus* egg extract in this molecular mass range. Several of our data are nevertheless contradictory to those of Shiina et al. (1992). These authors reported that p220 lowers the critical concentration for spontaneous MT assembly, in contrast to our results. Shiina et al. (1992) showed that p220 was not localized to MTs during mitosis whereas it was present on interphasic MTs. They also reported a ubiquitous expression of p220 in *Xenopus*. Using two mAbs we show that XMAP230 is not only localized to interphase but also to spindle MTs. We also find that XMAP230 is only present in proliferating cells, such as eggs, oocytes, testis and XL177 cells although an immunologically related 200-kD protein is present in other tissues. We do not think that this protein is a degradation product of XMAP230 because of the method of homogenization used.

XMAP230 is clearly different from XMAP215 previously purified by Gard and Kirschner (1987), which is not thermostable. XMAP230 shares some physical properties with MAP4 and an mAb raised against a thermostable protein from HeLa cells that had all the characteristics of MAP4 recognized XMAP230b (Faruki and Karsenti, 1994). Furthermore, the L5 mAb stained spindle MTs in HeLa cells (data not shown). However, four different anti-MAP4 antibodies (gift from J. B. Olmsted, University of Rochester, NY) did not recognize XMAP230. The appurtenance of these proteins to the MAP4 family remains therefore open. Although anti-MAP1B antibodies recognized XMAP230, peptide mapping revealed that XMAP230 and MAP1B are unrelated (data not shown). Furthermore, MAP1B antibodies stain the centrosome by immunofluorescence (Domínguez et al., 1994) whereas the L5 and L7 mAbs do not stain either isolated centrosomes or centrosomes in cells.

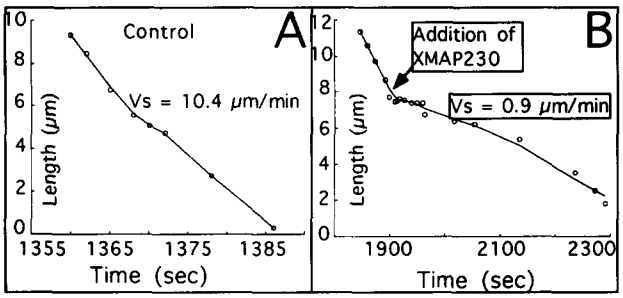

Figure 8. XMAP230 decreases v_s. MTs were analyzed during shrinkage in the absence (*A*) and presence (*B*) of XMAP230; *addition of XMAP230* denotes that new XMAP230 was added at that time point after perfusion with BRB80+1mM GTP; the time between shrinkage start and readdition of XMAP230 in *B* reflects the time needed for reinjection of XMAP230.

The effect of XMAP230 on MT dynamics is similar to the effect of the brain MAPs, tau and MAP2 (Drechsel et al., 1992; Pryer et al., 1992). This similarity suggests that the MT binding domain of XMAP230 is similar to that of tau and MAP2, a possibility also supported by the fact that they all bind to the same carboxy-terminal region of MTs as determined by subtilisin cleavage of MTs (data not shown). However, an important difference between brain MAPs and XMAP230 is the lack of effect on spontaneous MT assembly by the latter. It is possible that the egg contains tau-like proteins that directly promote spontaneous assembly as observed in interphase extracts.

Effect of XMAP230 on Microtubule Nucleation by Centrosomes

We have noticed two interesting effects of XMAP230 on MT nucleation. First, we determined that with the tubulin used in this study, the "critical" tubulin concentration for MT nucleation off centrosomes is close to 3 μM. At this concentration, XMAP230 did not facilitate MT growth off centrosomes. Using cryo electron microscopy, we have seen that MTs start to grow as sheets off the centrosomes before forming a tube (Chrétien, D., S. D. Fuller, and E. Karsenti, manuscript submitted for publication). The lack of effect of XMAP230 on the critical concentration for MT nucleation off centrosomes may mean that this MAP can bind only to fully formed MTs and not to initial nuclei. The other interesting observation is that as soon as the tubulin concentration is high enough to support MT growth off centrosomes, the number of MTs nucleated is dramatically increased by XMAP230. This is not due to binding of XMAP230 to the centrosomes, as preincubation of the centrosomes with XMAP230 followed by washing prior to the assay did not promote nucleation. The low number of MTs observed in the absence of XMAP230 is probably due to the incapacity of many MTs to reach a visible length before undergoing a catastrophe. Therefore the increased number of MTs nucleated in the presence of XMAP230 is most likely due to the MT stabilizing activity of XMAP230. These data confirm directly our previous proposal that soluble factors

not tightly bound to the centrosome, can regulate the number of MTs actually growing off a centrosome (Bré and Karsenti, 1990).

Localization and Function of XMAP230 During Mitosis

It is interesting to note that XMAP230 is localized to all MTs in interphase, seems to be released from MTs in prophase and reassociates with the mitotic apparatus in metaphase and anaphase, with the exception of astral MTs. Release of XMAP230 from MTs in prophase may be required for disassembly of the interphase array of MTs. An attractive speculation is that MAPs of this type are released from MTs in prophase to allow the effect of severing factors which are otherwise hindered by the presence of MAPs (Vale, 1991). The reassociation of XMAP230 with the MTs of the mitotic spindle seems paradoxical because XMAP230 is phosphorylated in vivo, and in vitro by cdc2 kinase and MAP kinase, and the phosphorylated protein seems to have decreased affinity for MTs (this paper and that of Shiina et al., 1992). Even more striking is the complete absence of XMAP230 from the astral MTs during metaphase and anaphase. One possible explanation is that XMAP230 is locally less phosphorylated around the chromosomes, perhaps due to the presence of a chromosomal type 1 phosphatase (Fernandez et al., 1992), allowing its specific binding to spindle MTs. If we assume that XMAP230 has a function in suppressing catastrophes during mitosis, this MAP may have an essential function by decreasing locally the value of f_{cat} around the chromosomes leading to a preferential relative stabilization of spindle MTs. This could explain how spindle MTs are stable enough to engage in an interaction with kinetochores and to form anti-parallel bonds at the spindle equator. Interpolar MTs were shown to be very stable (Mastronarde et al., 1993) and XMAP230 might be involved in their stabilization and crosslinking.

It is now clear that other non-neuronal MAPs should be identified in this way and their function in MT dynamics and in spindle assembly studied in vitro and by immunodepletion from egg extracts. In correlation with phosphorylation studies, this will bring the study of spindle morphogenesis from phenomenology to molecular characterization of the principles at work in this highly complex process.

The authors would like to thank all the members of the T. Hyman and E. Karsenti laboratories for moral support during this work. We thank J. B. Olmsted for the generous gift of the anti-MAP4 antibodies; T. Kreis for the anti-tubulin antibody. We also thank D. Chrétien for help with the video experiments; R. Heald for help with the centrosome and tubulin purifications; T. Hyman for many suggestions; and R. Heald, T. Hyman, and S. Reinsch for critical reading of the manuscript.

This work was partially supported by a European Union grant (ERB-CHBIT 930755) to S. Andersen, a short term Human Frontier Science Program (SF-120/92) and European Molecular Biology Organization (ASTF7188) Fellowship to J. Domínguez and a Human Frontier Science Program grant to E. Karsenti (RG-350/94).

Received for publication 7 April 1994 and in revised form 1 September 1994.

References

Allen, R. D., N. S. Allen, and J. L. Travis. 1981. Video-enhanced contrast, Differential interference contrast (AVEC-DIC) microscopy: a new method capable of analyzing microtubule-related motility in the reticulopodial network of allogromia laticollaris. *Cell Motil. Cytoskeleton.* 1:291–302.

Belmont, L. D., A. A. Hyman, K. E. Sawin, and T. J. Mitchison. 1990. Real-time visualization of cell cycle-dependent changes in microtubule dynamics in cytoplasmic extracts. *Cell.* 62:579–589.

Bloom, G. S., F. C. Luca, and R. B. Vallee. 1985. Identification of high molecular weight microtubule-associated proteins in anterior pituitary tissue and cells using taxol-dependent purification combined with microtubule-associated protein specific antibodies. *Biochemistry.* 24:4185–4191.

Bornens, M., M. Paintrand, J. Berges, M. C. Marty, and E. Karsenti. 1987. Structural and chemical characterization of isolated centrosomes. *Cell Motil. Cytoskel.* 8:238–249.

Bradford, M. 1976. A rapid and sensitive method for the quantitation of microgram quantities of protein utilizing the principles of protein-dye binding. *Anal. Biochem.* 72:248–254.

Bré M.-H., and E. Karsenti. 1990. Effects of brain microtubule-associated proteins on microtubule dynamics and the nucleating activity of centrosomes. *Cell Motil. Cytoskeleton.* 15:88–98.

Bré, M.-H., T. E. Kreis, and E. Karsenti. 1987. Control of microtubule nucleation and stability in Madin-Darby Canine Kidney Cells: The occurrence of noncentrosomal, stable detyrosinated microtubules. *J. Cell Biol.* 105:1283–1296.

Butner, K. A., and M. W. Kirschner. 1991. Tau protein binds to microtubules through a flexible array of distributed weak sites. *J. Cell Biol.* 115:717–730.

Domínguez, J. E., B. Buendia, C. Lopez-Otin, C. Antony, E. Karsenti, and J. Avila. 1994. A protein related to brain microtuble-associated protein MAP1B is a component of the mammalian centrosome. *J. Cell Sci.* 107:601–611.

Drechsel, D. N., A. A. Hyman, M. H. Cobb, and M. W. Kirschner. 1992. Modulation of the dynamic instability of tubulin assembly by the microtubule-associated protein tau. *Mol. Biol. Cell.* 3:1141–1154.

Evans, L., T. J. Mitchison, and M. W. Kirschner. 1985. Influence of the centrosome on the structure of nucleated microtubules. *J. Cell Biol.* 100:1185–1191.

Faruki, S., and E. Karsenti. 1994. Purification of microtubule proteins from *Xenopus* egg extract: identification of a 230 kD MAP4-like protein. *Cell Motil. Cytoskeleton.* 28:108–118.

Félix, M. A., P. R. Clarke, J. Coleman, F. Verde, and E. Karsenti. 1993. Frog egg extracts as a system to study mitosis. *In* The Cell Cycle, a Practical Approach. P. Fantes, editor. IRL Press, Oxford. 253–283.

Fernandez, A., D. L. Brautigan, and N. J. C. Lamb. 1992. Protein phosphatase type 1 in mammalian cell mitosis: chromosomal localization and involvement in mitotic exit. *J. Cell Biol.* 116:1421–1430.

Galfré, G., and C. Milstein. 1981. Preparation of monoclonal antibodies: strategies and procedures. *Methods Enzymol.* 73:1–46.

Gard, D. L., and M. W. Kirschner. 1987. A Microtubule-associated protein from *Xenopus* eggs that specifically promotes assembly at the plus-end. *J. Cell Biol.* 105:2203–2215.

Gliksman, N. R., S. F. Parsons, and E. D. Salmon. 1992. Okadaic acid induces interphase to mitotic-like microtubule dynamic instability by inactivating rescues. *J. Cell Biol.* 119:1271–1276.

Hirokawa, N., Y. Shiomura, and S. Okabe. 1988. Tau proteins: the molecular structure and mode of binding on microtubules. *J. Cell Biol.* 107:1449–1459.

Izant, J. G., J. A. Weatherbee, and J. R. McIntosh. 1983. A microtubule-associated protein antigen unique to mitotic spindle microtubules in PtK_1 Cells. *J. Cell Biol.* 96:424–434.

Kirschner, M., and T. Mitchison. 1986. Beyond self-assembly: from microtubules to morphogenesis. *Cell.* 45:329–342.

Laemmli, U. K. 1970. Clevage of structural proteins during the assembly of the head of bacteriophage T. *Nature (Lond.).* 227:680–685.

Mastronarde, D. N., K. L. McDonald, R. Ding, and J. R. McIntosh. 1993. Interpolar spindle microtubules in PTK cells. *J. Cell Biol.* 123:1475–1489.

Miller, L., and J. C. Daniel. 1977. Comparison of *in vivo* and *in vitro* ribosomal RNA synthesis in nucleolar mutants of *Xenopus laevis*. *In Vitro.* 13: 557–567.

Mitchison, T., and M. Kirschner. 1984*a*. Microtubule assembly nucleated by isolated centrosomes. *Nature (Lond.).* 312:232–237.

Mitchison, T., and M. Kirschner. 1984*b*. Dynamic instability of microtubule growth. *Nature (Lond.).* 312:237–242.

Murofushi, H., S. Kotani, H. Aizawa, S.-i. Hisanaga, N. Hirokawa, and H. Sakai. 1986. Purification and characterization of a 190 kDa microtubule-associated protein from bovine adrenal cortex. *J. Cell Biol.* 103: 1911–1919.

Murray, A. W. 1991. Cell cycle extracts. *Meth. Cell Biol.* 36:581–605.

Neant, I., and P. Guerrier. 1988. 6-Dimethylaminopurine blocks starfish oocyte maturation by inhibiting a relevant protein kinase activity. *Exp. Cell Res.* 176:68–79.

Parysek, L. M., J. J. Wolosewick, and J. B. Olmsted. 1984. MAP 4: a microtubule-associated protein specific for a subset of tissue microtubules. *J. Cell Biol.* 99:2287–2296.

Pryer, N. K., R. A. Walker, V. P. Skeen, B. D. Bourns, M. F. Soboeiro, and E. D. Salmon. 1992. Brain microtubule-associated proteins modulate microtubule dynamic instability *in vitro* real-time observations using video microscopy. *J. Cell Sci.* 103:965–976.

Shiina, N., T. Moriguichi, K. Ohta, Y. Gotoh, and E. Nishida. 1992. Regulation of a major microtubule-associated protein by MPF and MAP kinase. *EMBO (Eur. Mol. Biol. Organ.) J.* 11:3977–3984.

Ulloa, L., J. Avila, and J. Díaz-Nido. 1993*a*. Heterogeneity in the phosphorylation of microtubule-associated protein MAP1B during rat brain development. *J. Neurochem.* 61:961–972.

Ulloa, L., J. Díaz-Nido, and J. Avila. 1993*b*. Depletion of casein kinase II by antisense oligonucleotide prevents neuritogenesis in neuroblastoma cells. *EMBO (Eur. Mol. Biol. Organ.) J.* 12:1633–1640.

Vale, R. D. 1991. Severing of stable microtubules by mitotically activated protein in *Xenopus* egg extracts. *Cell.* 64:827–839.

Verde, F., J. C. Labbé, M. Dorée, and E. Karsenti. 1990. Regulation of microtubule dynamics by cdc2 protein kinase in cell-free extracts of *Xenopus* eggs. *Nature (Lond.).* 343:233–238.

Verde, F., M. Dogterom, E. Stelzer, E. Karsenti, and S. Leibler. 1992. Control of microtubule dynamics and length by cyclin A and cyclin B dependent kinases in *Xenopus* egg extracts. *J. Cell Biol.* 118:1097–1108.

Walker, R. A., E. T. O'Brien, N. K. Pryer, M. F. Sobeiro, W. A. Voter, H. P. Erickson, and E. D. Salmon. 1988. Dynamic instability of individual microtubules analysed by video light microscopy: rate constants and transition frequencies. *J. Cell Biol.* 107:1437–1448.

Walker, R. A., N. K. Pryer, and E. D. Salmon. 1991. Dilution of individual microtubules observed in real time in vitro: evidence that the cap size is small and independent of elongation rate. *J. Cell Biol.* 114:73–82.